https://doi.org/10.1016/j.cmpb.2022.107292

Fast NURBS-based Parametric Modeling of Human Calves with High-accuracy for Personalized Design of Graduated Compression Stockings

Xi Wang[1,2], Zongqian Wu[2], Ying Xiong[3], Qiao Li[4,5,*] and Xiaoming Tao[3,*]

[1]Engineering Research Center of Digitized Textile & Apparel Technology, Ministry of Education, Donghua University, Shanghai 201620, China

[2]College of Information Science and Technology, Donghua University, Shanghai 201620, China

[3]School of Fashion and Textiles, The Hong Kong Polytechnic University, Kowloon, Hong Kong, China

[4]Key Laboratory of Textile Science & Technology, Ministry of Education, Donghua University, Shanghai 201620, China

[5]College of Textiles, Donghua University, Shanghai 201620, China;

Corresponding authors:

Qiao Li, qiaoli@dhu.edu.cn

Xiaoming Tao, xiao-ming.tao@polyu.edu.hk

Abstract:

Background and Objectives:

Accurate human body models are increasingly demanded by high-quality human-centered ergonomic applications, especially the design and manufacturing of compressive functional apparels. However, existing parametric models in related works are not capable to accurately describe detailed local shape features of human.

Methods:

In this work, a high-accuracy parametric modeling approach for human limb was proposed. 3D Scans of human calves were studied. Key data points of the scanned human calves were identified according to human anatomy, forming a quasi-triangular mesh of feature points. Then, non-uniform rational B-splines (NURBS) method was implemented. Control points were calculated from the key data points, with which the human calf shapes can be reconstructed by the smooth NURBS surface, giving rise to a new parametric model of human calves. Error between the scanned and reconstructed calf shapes were analyzed to verify the effectiveness of this model.

Results:

Error analysis showed that, this proposed method delivers a high-efficiency and high-accuracy parametric shape modeling approach with averaged error observed as only 0.37% for all the 260 subjects, much less compared to previous relative works (around 5%). For tentative application, customized medical compression stockings were designed based on this model and proved as valid to exert desired gradient compression on the according calf mannequin.

Conclusions:

By introducing the non-uniform rational B-splines method, a parametric model capable of characterizing human limbs with high-accuracy was proposed. Using very small amount of data, this model is expected to highly facilitate remote customized design and provide 3D shape references for design of compressive garments. Moreover, the proposed methods can inspire developments of other mixed modeling methods for high-accuracy applications.

Keywords: NURBS; parametric modeling; human calves; high-accuracy

1.Introduction

Critical individual fitness as well as precise functional performance have been

pushing the need for high-quality human-centered design, giving rise to a strong market trend of personalization nowadays. To this end, accurate human body models are increasingly demanded, especially in the research areas of apparel manufacturing, ergonomic applications, virtual try-on, and computer vision [1-4]. Consumers today prefer high-quality fashion products designed according to detailed body shapes for favorable fitness [5]. Virtual ergonomic assessment are also demanding precise shapes to evaluate try-ons prior to product manufacturing [6, 7]. Things become even more severe when it comes to compressive functional garments. Being used for orthopedic supports, compression therapy, etc., compression garments require precise description of target body part in order to provide desired functions [8-10]. Take the graduated compressive stockings (GCS) in physical therapy of chronic venous insufficiency (CVI) for example, critical graduated pressure distribution on human calves is required to facilitate venous return and relief venous reflux [11, 12]. However, the standards regulating size design and size selection of GCS, i.e., Medical Compression Hosiery European Pre-standard ENV 12718, Germany standard RAL-GZ387 and British standard BS:6612, are based on target populations' statistical distribution of leg circumferences only [13, 14]. In other words, only averaged compressions other than localized can be guaranteed. Thanks to the irregular shape of human calves and insufficient consideration of calves' 3D morphology details in those standards, risks of misuse remains one of GCS' largest challenges, leading to aggravation of symptoms instead of alleviation [15].

In order to address the above and similar problems, the 3D scanning technologies have been widely used to produce direct accurate 3D models for categorization [16], fit analysis for apparel design [17, 18], finite element analysis to evaluate compression mapping [19, 20], as well as body measurements [21, 22]. Normally, massive data are required to represent detailed shapes, increasing both processing cost and application cost. In

response to this, various template model-based scaling models have been proposed [23-26], which introduced several registered key parameters to construct target shapes. However, very few works on accurate parametric models of human shapes for fit design of apparels can be found in literature [23, 27]. For instance, the extensively-implemented surface registration technologies seek to achieve optimized geometric accordance of modeled surfaces, but for low-accuracy scenarios only and hence mainly used in shape morphing, hole-filling as well as surface transferring among various scans or different poses[24, 28-30]. This can also be confirmed in literature as well as according to the trace of the world-class digital human modeling (DHM) conferences in last decades. Besides, although some models chose anatomy-based features as key parameters, the determination of those features was generally based on statistical scope of shape variations [31], making the model only able to describe general features instead of detailed localized ones. To fundamentally solve this dilemma, it's better to place major concerns on the detailed shape other than model adaptation, i.e., determine the features for individual at most according to anatomy, then introduce an all-purpose shape/surface to fit all the features.

Hence in this work, a high-accuracy parametric model of human calves for safety customization of GCS is to be proposed. Scanned human calves were studied, and key data points identified the according to human anatomy, so that all scanned shapes can be parameterized. Then, instead of using surface registration technologies, we opted to compute the control points of the calf contours and apply the non-uniform rational B-splines functions (NURBS) [32-35], which are naturally smooth surfaces yet with capability of excellent irregular detail representation[36, 37], to fit features points to the calf shapes. Finally, accuracy and efficiency of this modeling approach are to be evaluated through error analysis of the reconstructed shapes compared to origin scanned ones, as well as try-on of the remote designed GCS assisted by the model on

according calf mannequin. This paper aims at proposing a new parametric 3D parametric model with high-accuracy based on key position labeling on human body and the NURBS method. The result not only provides a high-efficiency and accurate parametric model for human limbs, but will also inspire developments of other mixed modeling methods for high-accuracy applications.

2.Methods

The overall flowchart of this work can be depicted in **Figure 1**, which compromises 5 parts in sequence, i.e., circumference profile analysis, curvature analysis, knots computation, NURBS mech construction and error analysis.

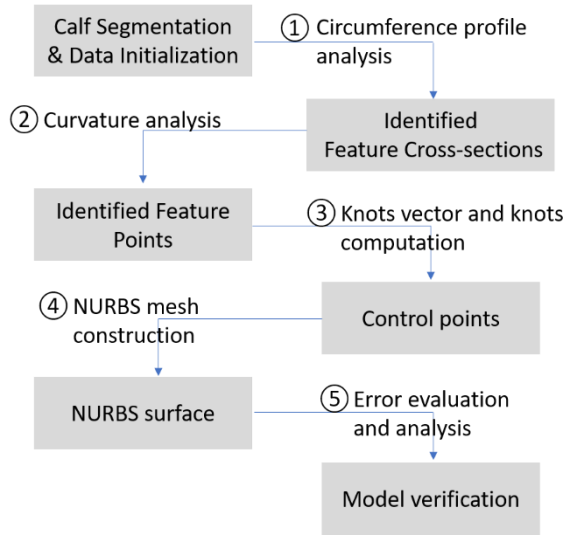

Figure 1 Schematic diagram of the NURBS modeling of human calves

2.1 Data acquisition and initialization

Details of 3D acquisition setup and process can be found in our previous work elsewhere [25]. Briefly, NX-16 automatic full-body scanner ([TC]^2, NC, USA) were used to acquire full-scale 3D human shapes with a scanning resolution of 5 degrees in the circumferential direction and 1 mm in the height direction. 3D

scans of total 260 subjects (China residents) were obtained in this research, with 175 females and 85 males, of which about 92% were middle-aged or older, reported as major sufferer of CVI disease. Clinical diagnosis prior to this study showed that about 61% of all subjects were already with varicose vein symptoms on one or both legs, hence proper to be target subjects for studying design of fitted MCS.

To have the calves isolated from the scanned whole-body shapes, segmentation was conducted based on human anatomy characteristics. Upper limit of tibia and lower limit of fibula can be easily identified according to local bulge and sag, between which the middle regions were retained as the calf sections. Principal component analysis was applied on each extracted calf to calculate its general orientation, based on which the inclined calf can be rotated to upright position for simpler circumference calculation later. Details of those segmentation and orientation standardization can also be found in our previous work [25].

Since original scanned dots were in irregular arrangement and difficult to arrange, a gridding resampling process was further implemented, including contour determination and 2D polar resampling. A set of equidistant parallel planes (distance between was the same as resolution of origin scanned data) were used to intersect with origin dot cloud. For each slicing plane, the nearest dots-pairs or dots on the plane giving the 2D contour of cross-section (**Figure 2**). Then, the 2D contour was then transferred to the polar coordinate system, in which curve fitting was introduced to get the explicit shape of the contour. This correlation coefficients were observed as high as 0.9999 since no shape distortion was introduced for this step. For each contour curve, dots were further sampled every 5 degrees around the weight center, by which means a new calf model representation using parallel cross-sectional contours can be obtained. Easy to understand that this resampling process maintained the same resolution as the origin.

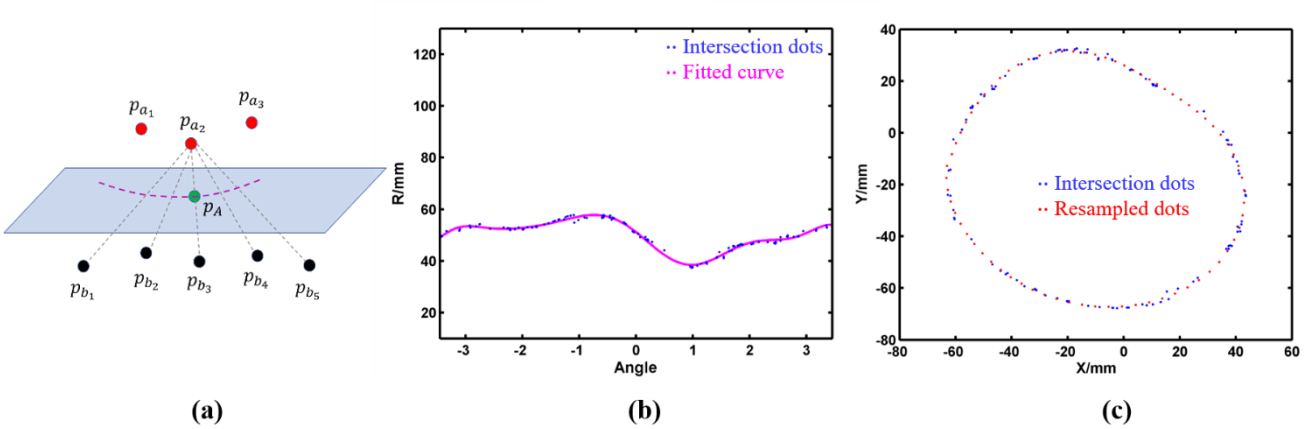

Figure 2 Slicing and resampling: a) Contour determination: p_{a_2} and p_{b_3} are one of the nearest dot-pairs, through which the intersection p_A and others constitute the contour of cross-section; b) Intersection dots were fitted in polar coordinate system, from which new dots were resampled evenly; c) Comparison of intersection dots on contour and the resampled dots.

2.2 Circumferential profile analysis: identification of feature locations

A circumferential profile $C(h)$ is the height-circumference relationship of a human calf, which is the essential characteristics for MCS size design and selection as elaborated in standards such as GAL-GZ387/1. The feature locations of a human calf are B, B1, C, and D, who corresponding in anatomy to the ankle, junction of gastrocnemius and ligaments, maximum thickness of gastrocnemius, and tuberositas tibiae. According to this definition, B, C and D can be easily identified as the local minimum and maximum of a circumferential profile (**Figure 3a**). As per B1, although the transition from ligaments to gastrocnemius is usually smooth and not quite significant, the thickness increasing of gastrocnemius up to muscle belly shall be much quicker than that of tendon. In other words, the feature height B1 can be conveniently identified as local maximum between B and C, via study of $C'(h)$ (1st order derivative of circumferential profile, **Figure 3b**). In consideration of the anatomic location of the 4 feature locations, the authors used a speedup strategy: First, search for the local maximum value within the range of calf.

This will provide the location of the gastrocnemius belly at maximum thickness (C). Then, find the nearby 2 local minimum lower and higher than C, giving the smallest circumference around the ankle (B) and that below the tuberositas tibiae (D). Finally, the connection point of tendon and the gastrocnemius (B1) can be found as the local maximum of 1st-order derivative of circumferential profile between B and C.

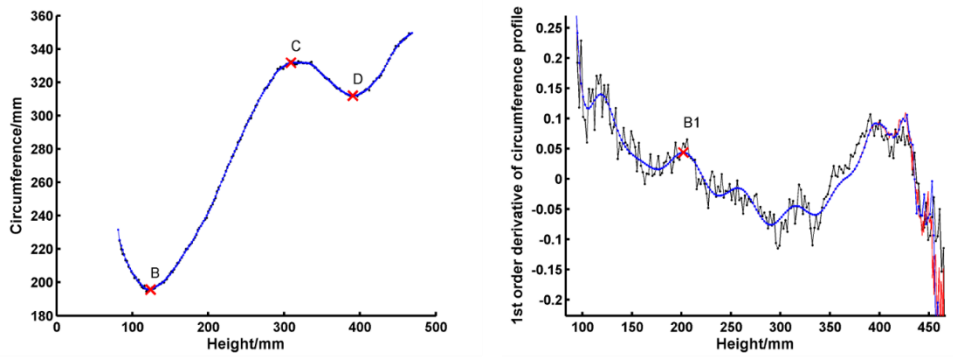

Figure 3 Feature locations identification: **(a)** B, C and D of human calf can be observed from circumferential profile, while **(b)** B1 can be identified from 1st order derivative of circumferential profile.

2.3 Curvature analysis: identification of feature points

With feature parallel contours obtained, feature points can then be identified through analysis of the contour shape at the feature locations. For further construction of NURBS modeling, those feature points shall largely reflect the shape characteristic. Concretely for a smooth closed curve like the circumferential contour, the 'sharp' (local curvature maximum) and 'blunt' (local curvature minimum) locations around decide the contour shape. Here we incorporate a most simple method of finding the points around the 2D cross-sections through analysis of curvature.

Firstly, the contour curve in polar coordinate system ($r - \theta$ curve) was

searched for peaks and valleys, the corresponding data point of which were recorded as point set S1. Then, angle intervals with little variation of radius were found, while the middle points of those intervals were recorded as point set S2. This step is to prevent some arc-shaped regions to be distorted by further curve-fitting. Thirdly, curvature distribution of the contour was analyzed, and the local peaks and valleys of curvature were recorded as another type of characteristic locations of the contour (S3). Moreover, middle points between characteristic locations and within larger spans in point set S3 were specially retained. Before those key dots can serve as feature data points in the computation of knots in NURBS modeling, a re-arrangements process shall be conducted. The 3 types of point sets of all contours **(Figure 4a)** were merged and classified into certain number of clusters by K-means clustering algorithm (**Figure 4b**). This procession ensures all feature points can form a quasi-rectangular mesh, which is best for the efficiency of NURBS fitting.

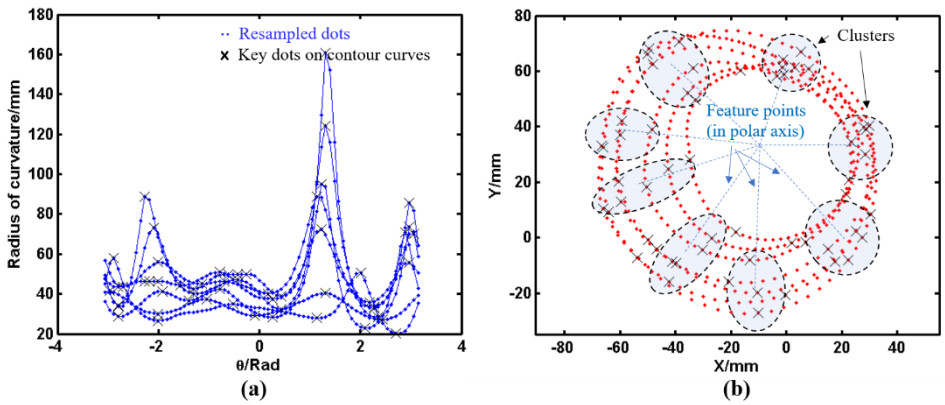

Figure 4 Feature points identification: a) Key points observed from curvature analysis of 2D cross-sectional contours, and b) Clustering of key points to have feature points (8 centroids case)

Moreover, although the overall shapes of human calves are smooth and the selection of feature locations are based on standards, the shape between heights cannot be sufficiently expressed by one blending functions. Hence, to improve accuracy of NURBS modeling, middle cross-sections between neighboring

feature locations were additionally enrolled, lead to a 7-layer structure. For this work, the localized curvature was calculated based on a 5-point circle fitting method, of which the number of enrolled points controls the accuracy of the curvature distribution.

2.4 Control points calculation

NURBS (non-uniform rational B-splines) is a well-known convenient way in computer-aided design area to represent smooth curves or surfaces, while simultaneously provide easy in-location manipulation via adjusting corresponding control points. The NURBS modeling requires control points, knots vectors and weights to construct continuous shape, thus retains in nature the favorable compactness, uniformity, as well as economies of storage and transmission. Those merits well explain the rationales of this work using NURBS for high-accuracy modeling of human calves.

According to definition, any NURBS surface can be given by

$$p(u,v) = \frac{\sum_{i=0}^{m}\sum_{j=0}^{n} N_{i,p}(u)N_{j,q}(v)w_{i,j}c_{i,j}}{\sum_{i=0}^{m}\sum_{j=0}^{n} N_{i,p}(u)N_{j,q}(v)w_{i,j}} \quad (1)$$

where $c_{i,j}$ is the rectangular mesh of control points, $w_{i,j}$ is weights to tune the distance between control points and the surface, $N_{i,p}(u)$ and $N_{j,q}(v)$ are the NURBS blending function along the knot vector u and v in the 2 directions of the mesh:

$$N_{i,0}(t) = \begin{cases} 1, & if\ t_i \le t \le t_{i+1} \\ 0, & otherwise \end{cases}$$

$$N_{i,p}(t) = \frac{t-t_i}{t_{i+p}-t_i} N_{i,p-1}(t) + \frac{t_{i+p+1}-t}{t_{i+p+1}-t_{i+p}} N_{i+1,p-1}(t) \quad (2)$$

in which t_i is element of knot vectors. while knot vector u and v can be determined via Hartley-Judd equation. This leaves a most essential task of determining the control points based on the data points. To facilitate the modeling process and save computation, here we opted to use another efficient

scheme. Instead of computing control points for the surface, we calculate control points for contour curves of each feature cross-section, and use them as the set of control points for the NURBS surface. Since human calves approximately appear in cylindrical shape, this simplification is expected to not cause much distortion.

To build cubic NURBS curves with m data points ($d_0 \sim d_{m-1}$) for the closed contour curves of the featured cross-sections, 4 repeated cycle vertices shall be added, i.e., $d_0 = d_m; d_1 = d_{m+1}; d_2 = d_{m+2}; d_3 = d_{m+3}$. The knot vector U is then $[u_0, u_1, \dots, u_{m+3}]$, where elements $u_3 \sim u_{m-1}$ for inner knots $d_3 \sim d_{m-1}$ can be determined via normalized accumulated chords according to Hartley-Judd equation. Since all the nodes shall be on the NURBS curve, this would lead to m equations, which can be further expressed by a simple matrix equation:

$$\begin{bmatrix} b_1 & c_1 & & & & a_1 \\ a_2 & b_2 & c_2 & & & \\ & & \ddots & \ddots & \ddots & \\ & & & a_{m-2} & b_{m-2} & c_{m-2} \\ c_{m-1} & & & & a_{m-1} & b_{m-1} \end{bmatrix} \begin{bmatrix} \boldsymbol{d_1} \\ \boldsymbol{d_2} \\ \vdots \\ \vdots \\ \boldsymbol{d_{m-2}} \\ \boldsymbol{d_{m-1}} \end{bmatrix} = \begin{bmatrix} \boldsymbol{e_1} \\ \boldsymbol{e_2} \\ \vdots \\ \vdots \\ \boldsymbol{e_{m-2}} \\ \boldsymbol{e_{m-1}} \end{bmatrix} \quad (3)$$

where

$$\begin{cases} a_i = \dfrac{(\Delta_{i+2})^2}{\Delta_i + \Delta_{i+1} + \Delta_{i+2}} \\ b_i = \dfrac{\Delta_{i+2}(\Delta_i + \Delta_{i+1})}{\Delta_i + \Delta_{i+1} + \Delta_{i+2}} + \dfrac{\Delta_{i+1}(\Delta_{i+2} + \Delta_{i+3})}{\Delta_{i+1} + \Delta_{i+2} + \Delta_{i+3}} \qquad i = 1 \sim m-1, \Delta_i \\ c_i = \dfrac{(\Delta_{i+1})^2}{\Delta_{i+1} + \Delta_{i+2} + \Delta_{i+3}} \\ \boldsymbol{e_i} = (\Delta_{i+1} + \Delta_{i+2})\boldsymbol{d_{i-1}} = u_i - u_{i-1} \end{cases}$$

With selected feature points fed into this matrix equation as data points, the control points for contour of each feature cross-section can be given. It's should be pointed out that, to facilitate the fitting process, we opt not to directly

calculate the control points set for the 3D surface. Instead, control points of 2D contours are to be calculated, which constitute one of the control points sets among all feasible ones to describe the target surface. Worth-mentioning that, through proper arrangement of the nodes using k-means method above, the collection of control points for contours makes an effective set of control points to be further utilized to construct the 3D NURBS surface of human calves. By doing so, calculation can be largely reduced, speeding up the modeling process.

2.5 NURBS surface construction

According to the above equation, once the control points are obtained, explicit expression of the NURBS surface can be determined. The same number of data points among different feature cross-sections leads to same number of control points, which can be formed into a rectangular mesh:

$$[c_{i,j}] \quad i = 1{\sim}7, j = 1{\sim}m$$

where $c_{i,j}$ is the *j*th control point of the *i*th layer, i.e., each row conveys control points for certain contour of 'latitude cross-section' (u-direction), while each column contains control points for each 'longitude cross-section'(v-direction).

Knots vectors of the data points are further required. Based on data points corresponding to the above mesh of control points, both knots vector matrix u and v can be calculated as the averaged knot vector in u-direction and v-direction.

Further to show this surface, for any pair of (u, v) selected on certain sampling frequency, the point at the NURBS surface can be determined and plotted. For this part, authors acknowledged and implemented the NURBS toolbox by D.M. Spink [38].

2.6 Verification: error analysis

To test the validity of this series of method on providing a high-accuracy modeling of origin calves, the error between the constructed NURBS surface

and origin scanned dots cloud shall be evaluated. In fact, although the NURBS modeling can be considered as a transformation of coordinates from u, v to cartesian coordinate system, the resultant curves/surfaces are actually continuous shapes. Though there is well-accepted published works on calculating the distance between an out-plane data point and a continuous NURBS surface [32, 39], here we use a fast but efficient 2-step scheme.

First, the determined NURBS surfaces of human calves were resampled on a sampling rate with denser resolution compared to the origin scanned dot cloud. In this scenario, the NURBS surface can be approximated by a set of quadrilateral surface elements with corners $P_{i,j}, P_{i+1,j}, P_{i+1,j}$ and $P_{i+1,j+1}$, where Ps are the resampled points from the NURBS surface. It's not necessary for those 4 corners to be in one plane, though they will finally be when the sampling rate is high enough. Either way, the quadrilateral surface can be further approximated by two adjacent planes determined by 3 corners each. For instance, quadrilateral surface with corners $P_{i,j}, P_{i+1,j}, P_{i+1,j}$ and $P_{i+1,j+1}$ can be approximated by triangular planes with $P_{i,j}, P_{i+1,j}, P_{i+1,j+1}$ and $P_{i,j}, P_{i,j+1}, P_{i+1,j+1}$. By doing so, the error of the NURBS surface from origin dots can be indexed by the overall distance between origin dots and the triangular plane elements.

Secondly, for any out-plane dot $\boldsymbol{q}$, its nearest corner $\boldsymbol{g_{x,y}}$ can be located through searching the minimum point-to-point distance between $\boldsymbol{q}$ and all corners. The 4 neighboring corners $\boldsymbol{g_{x-1,y}}$, $\boldsymbol{g_{x,y-1}}$, $\boldsymbol{g_{x,y+1}}$and $\boldsymbol{g_{x+1,y}}$ (**Figure 5**) belong to the consecutive adjacent 2×2 triangular planes centered by $\boldsymbol{g_{x,y}}$ can be further picked out. Easy to prove that the nearest distance between $\boldsymbol{q}$ and the 2×2 triangular plane matrix approaches the distance between $\boldsymbol{q}$ and NURBS surface as sampling rate increases. For each element in the 2×2 triangular plane matrix, point-to-plane distance was calculated and the minimum distance l was recorded as the approximation of distance error

between origin scanned dot $\boldsymbol{q}$ and the NURBS surface (**Algorithm 1**).

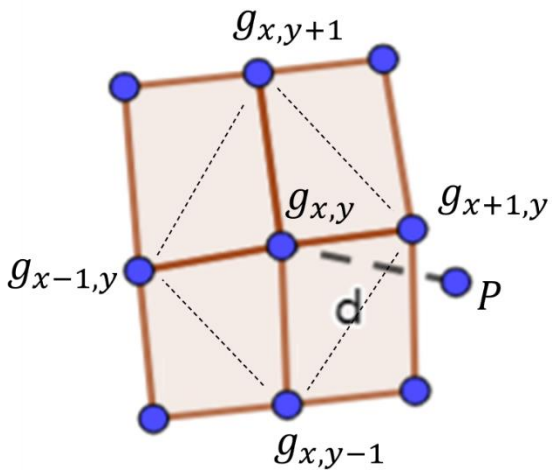

Figure 5 Error of NURBS surface to original scanned dot *P*, where $g_{x,y}$ is the nearest point in NURBS surface, while $g_{x-1,y}$, $g_{x+1,y}$, $g_{x,y-1}$, $g_{x,y+1}$ are neighboring corners.

Algorithm 1: Computing error of a single dot from the NURBS surface

---

Input: originally scanned single dot p, NURBS surface patch with vertices set $V=(v_1,\ldots v_n)$

Output: error of a single dot from the NURBS surface

1: $D = (|p- v_1|,\ldots(|p- v_n|)$; //Distances vector of p to vertices V
2: min(D) = |p- F|; //Search the nearest dot to p
3: **if** length(F)=1 **then**
4: S1=BCFG, S2=CDEF, S3=GFIH, S4=EFIJ;
5: $d = (d_1 ,d_2 ,d_3 ,d_4)$;// point-to-surface distance of p to S1~S4
6: Return min(d);
7: **else**
8: $N = (n_1 ,n_2 ,n_3 ,n_4)$; //number of nearest vertices for S1~S4
9: Max(N) = n_j; //determine nearest surface patch
10: Return point-to-surface distance of p to S_j;
11:**end if**

To provide a nondimensionalized overall discrepancy of the NURBS surface from origin scanned dots, for this work, all distance errors ls shall be considered. Since there are differences in circumferential size between contour curves of different cross-sections, error l to the origin scanned dot shall be normalized by a size indicator, which is selected as the averaged diameter in this work. Now the overall error can be given by the root mean square of all normalized errors:

$$E = \sqrt{\frac{1}{kh_k}\sum_k \sum_{h_k} \left(\frac{l_{kh_k}}{r_k}\right)^2} \tag{4}$$

where k is the number of cross-sections, h_k is the number of scanned dots on current layer, r_k is the averaged radius of cross-sectional contour. The error index E will give an overall characterization of the shape distortion between origin dots cloud and the constructed NURBS surface.

3.Results

To demonstrate the modeling process and intermediate results, left calf of subject No.43 was randomly selected. For the error analysis, calves of all subjects were statistically analyzed.

3.1 Data acquisition and initialization

A typical demonstration of the segmented calf from original scanned shape, upright-placed scanned calf, and griding resampled calf are summarized and shown in **Figure 6.** As aforementioned, the resampling density was 200 in height direction and 72 in circumferential direction, higher than density of origin scan. Before that, it's observed that the coefficients of determination R^2 were all higher than 0.9993 for all fitted contour curves, showing that the resampling process introduced ignorable shape error.

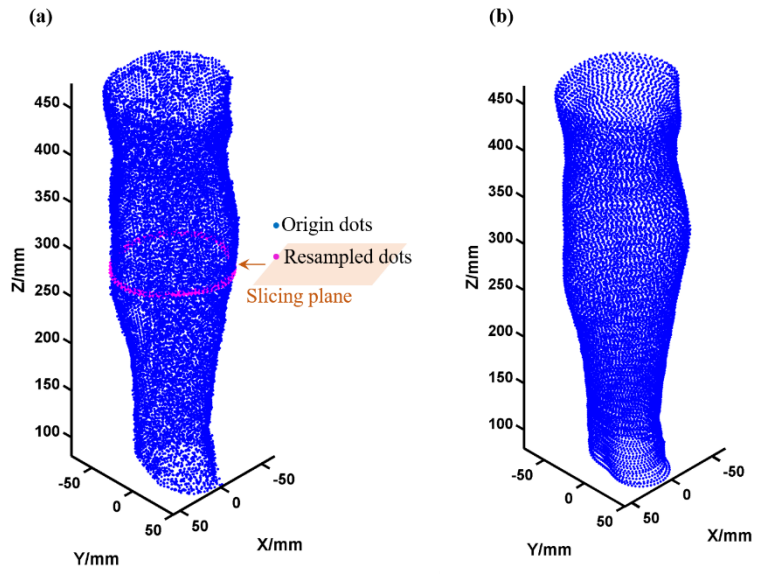

Figure 6 The resampled calf shapes: intersects dots by slicing plane were fitted according to **section 2.1**, from which new dots were sampled, giving the smooth resampled calf shape as in (b).

3.2 Identification of feature locations and feature dots

For each cross-section of the resampled calf, the circumference can be computed as the accumulated length of chords between adjacent points. Circumferential profile can then be easily calculated, from which the feature locations B, B1, C and D can be easily identified according to **section 2.2**. A typical demonstration of the identified location of B, B1, C and D is plotted in **Figure 7a**, while **Figure 7b** showed the total 7 feature cross-sections of the resampled calf.

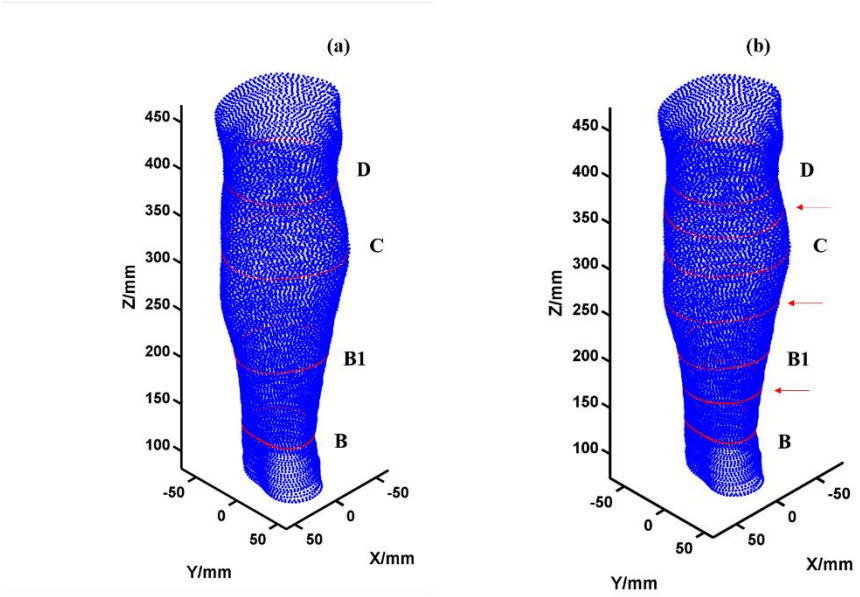

Figure 7 Identification of feature locations: B, C and D can be identified in circumferential profile while B1 can be determined from the 1st order derivative of circumferential profile (a). 7 feature locations with 3 more intermediate cross-sections were also picked to enhance the modeling accuracy (b).

With 72 data points for each contour of the feature cross-sections, fitted NURBS surface of human calf can be built. However, to balance between computation efficiency and modeling accuracy, this work tended to use only the crucial data points that defined the trend of the contours. Although the k-means distortion figure (**Figure 8a)** showed that 8 centroids can successfully categorized all feature points, 15 centroids was further used for comparison of accuracy in following section, leading to 7*8 and 7*15 rectangular mesh matrix, respectively. Feature points were then calculated according to the matrix, as shown in **Figure 8b**.

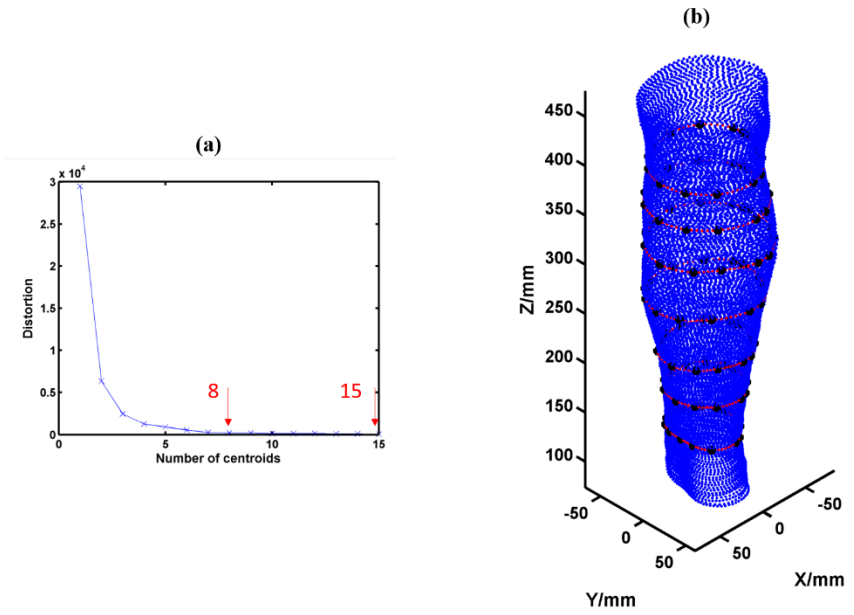

Figure 8 Feature points identification using k-means. The k-number can be determined in (a), and the 7*15 identified feature points for NURBS modeling can be seen in (b).

3.3 NURBS modeling

With all feature data points obtained, the control points of each contour can be calculated, as plotted in **Figure 9a**. Easy to see that all control points were on the same plane as data points. Node vector in u-direction and v-direction can also be computed.

With node vectors and the control points arranged in rectangular mesh, the NURBS surface can be finally determined (**Figure 9b**). **Figure 9c** demonstrates a typical comparison of scanned shape and the NURBS surface of human calf for a randomly chosen subject. Worth-mentioning that resultant NURBS surface was actually a continues surface, but exhibited in only 100×100 density here.

It can be observed that the NURBS surface generally accords with the origin scanned data. To quantify the difference between those 2, error of the NURBS

surface shall be computed and analyzed.

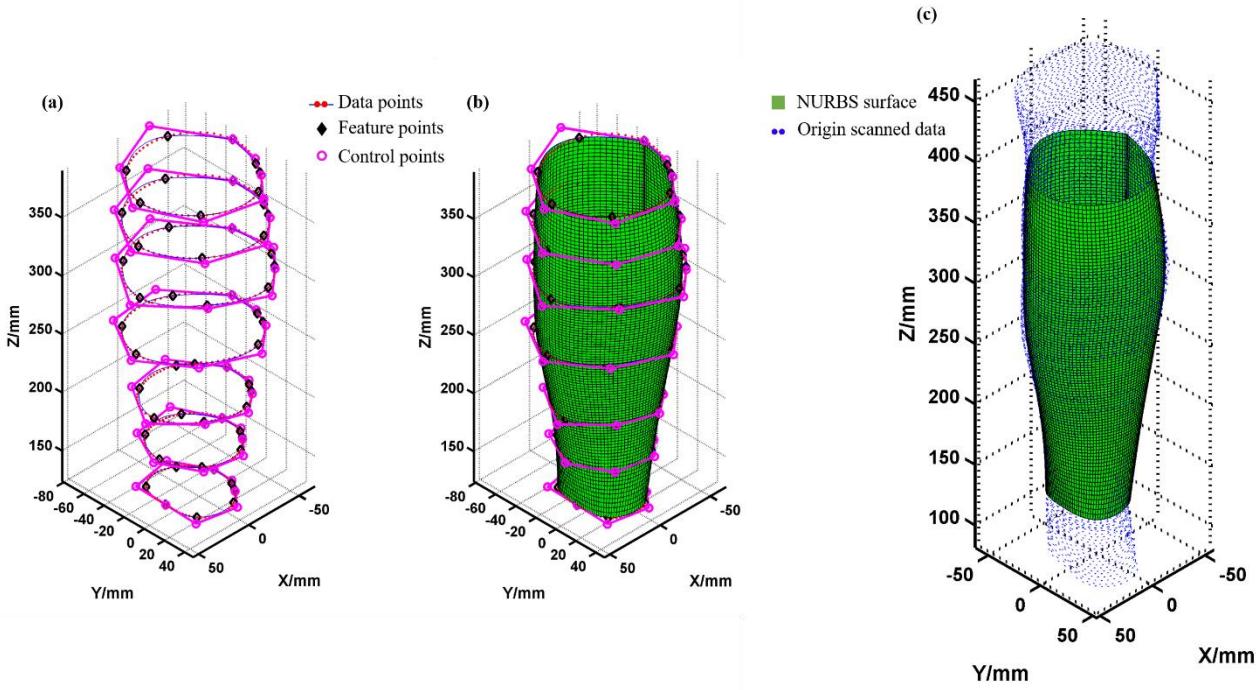

Figure 9 NURBS modeling. Control points can be calculated according to the obtained feature points (a), which can be further used to build NURBS surface (b) and compared to origin scanned shape (c).

3.4 Error of the NURBS-based calves

Based on the proposed algorithm in **section 2.6**, error index of a fitted NURBS surface from the origin scanned data can be calculated. In this work, accuracies were compared between sparse and denser feature points mesh, i.e., the 7*8 feature point matrix and 7*15 feature points matrix. Finally, the error between the reconstructed NURBS surface and the origin scanned data were evaluated and plotted in **Figure 10**.

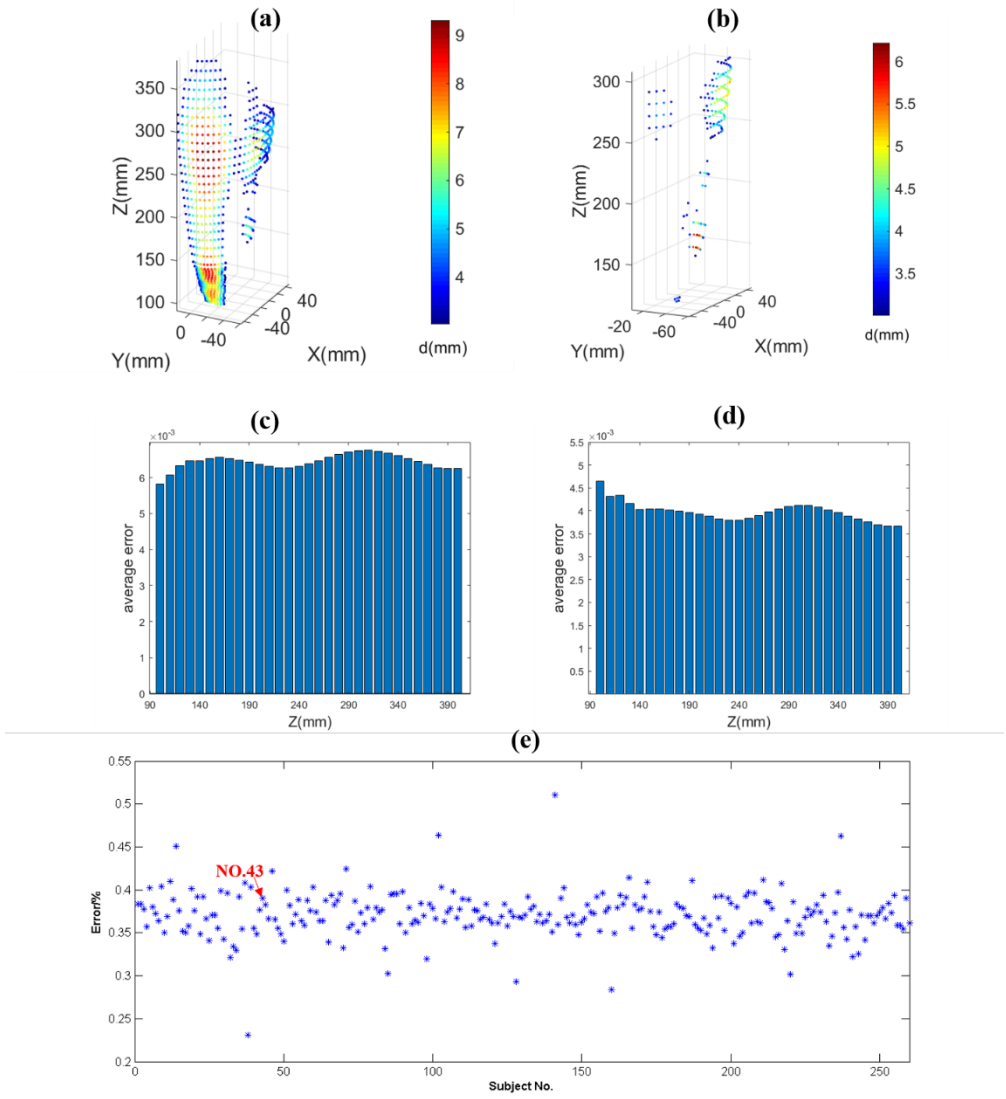

Figure 10 Error of the NURBS surface. (a) and (c) depict data with distance discrepancy higher than 3mm, as well as the averaged error for subject No.43 when using the 7*8 mesh. (b) and (d) reveal another case with finer mesh of 7*15 feature points. (e) shows the error distribution of NURBS surface constructed with finer mesh for all the 260 subjects.

It can be observed in **Figure 10** that larger errors generally happened at the location of B1 and that below D, indicating that the special anatomy structure

with calcaneal tendon and diverse knee shape largely added into the complexity of local shapes, which made the re-arrangement of data points less reliable. The averaged error of the NURBS modeling with sparse mesh of 7*8 feature points can be found with a small value of only 0.63%. The maximum error was about 9.15 mm around the B1 location. For the other case with finer mesh of 7*15 feature points, the error can be further reduced to 0.39%, with maximum error of 6.22 mm around B1 location. This result showed that finer mesh of feature points provides much more accurate modeling of human calves. Moreover, for all the 260 subjects, the errors of the NURBS modeling with finer feature points were observed as low as 0.37%±0.03%, which verified this effective shape parametric modeling as a high-accuracy modeling approach, with minimal averaged error among relative works, and about an order of magnitude less than around 5% as in previous work [25].

4.Application

Before further applications of using this model for high-accuracy personalized design scenarios, a preliminary attempt of using the modeling approach for design of gradient medical compression stockings was conducted. The averaged calf of subjects was analyzed for feature locations and points, based on which the whole calf can be reconstructed, and sent to factory for 3D printing (printing material: silicone type 903) and also to MCS designer for a customized half-height gradient MCS. The MCS designer considered the mechanical stiffness of fabrics, crucial locations as well as the localized radius of curvature, according to which the target compression can be determined, through

$$P = \frac{K\varepsilon}{r}$$

where K is the tensile stiffness per unit width, ε is the strain of stockings

around selected location, r is localized radius of curvature. The fabricated customized half-height MCS was then worn on the calf mannequin, on which pressure were measured for B, B1 and C locations to verify the design, as in **Figure 11**.

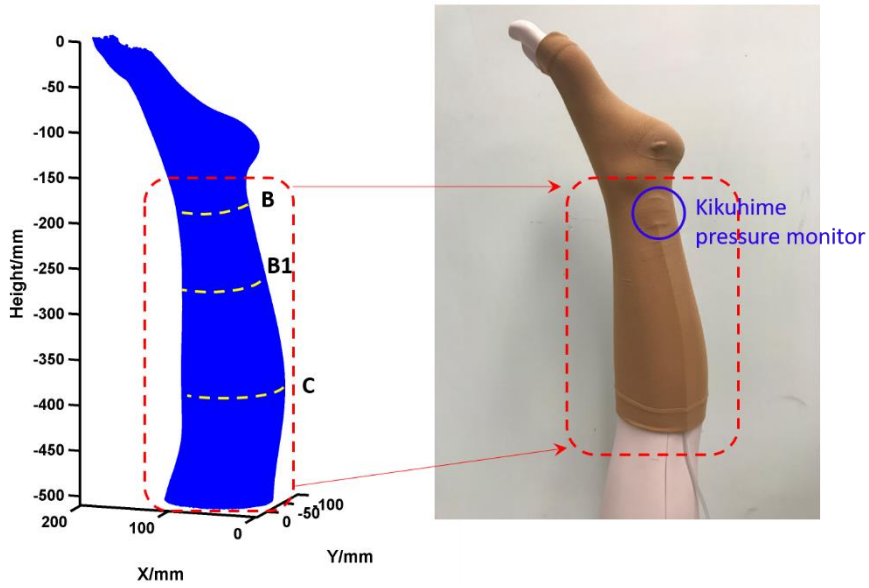

Figure 11 Pressure validation of MCS on the mannequin made NURBS-based modeling

Table 1 measured pressures (kPa) of the customized MCS on the mannequin.

Orientations\locations	B	B1	C
Inner	2.527±0.000	2.261±0.077	1.729±0.077
Outer	3.724±0.077	2.66±0.000	2.128±0.000
Front	4.256±0.077	3.192±0.133	2.261±0.077
Rear	4.788±0.133	2.793±0.077	2.128±0.000

The measured pressures were summarized in **Table 1**. Easy to see that for all the 3 locations, the compressions on B, B1 and C revealed clear gradient trends

($P_B > P_{B1} > P_C$), which validated this customized design and the high-accuracy modeling approach proposed in this work. It can also be observed from **Table 1** that, due to irregular circumferential shapes, there were significant differences among orientations, especially for B front and B rear where tendons bulged and affected the shapes. This indicated indirectly that the other customized designs based on anthropometric measurements only cannot guarantee safety compression on skin, and therefore a high-accuracy model for precise design shall be implemented in future.

5.Discussion

Instead of achieve high model adaption among a population, this work tends to using the well-accepted features to provide a human parametric model with individual shape details with high accuracy to the origin shapes. Other than solving the affine transformation between sets of landmarks, it's also promising to place major focus on feature points extraction and implement efficient tools to curve-fit the surface. Using this approach, not only a high-accuracy model of the origin can be obtained (with error of mere 0.37% as indicated in result section, best achievement to the state-of-the-art), the feature points can also be kept or analyzed for other applications, such as the motion recognition.

As per the error distribution in **Figure 10e**, No.38, 128, 85, 160 and 220 were observed with minimal error of less than 0.3%, while No.14, 46, 71, 102, 141 and 237 were observed with maximal errors of higher than 0.42%. Double check on the scanned shapes showed that, those with small errors belonged to young subjects with cylindrical calves, which best fit the requirement of NURBS method. Meanwhile, those with larger errors were observed either with severe CVI symptoms on calves, making the surface badly uneven and not ideal for the NURBS-based modeling, or bony and with curved tibia, which dominate the calf shale in a more irregular way.

It should be pointed out that, to simplify and speed up modeling process, the control points were calculated for the contour of each cross-section, but taken as that of the surface. Furthermore, averaged knot vectors in both *u*,*v* directions were utilized to fit the feature points. Authors are aware of that, according to the theory of NURBS, this speeding up schemes would exert additional requirements on the quasi-rectangle grid of points for NURBS surface fitting. For example, all contours of cross-sections shall be similar figures to achieve perfect accordance. This, however, cannot be satisfied for irregular human contours along the direction of length. In this work, authors introduce more features (intermediate planes between feature ones, as well as more centroids/feature points) to balance the error. Results showed that this scheme was successful to provide a high-accuracy but fast parametric model.

For preliminary application, it's shown that a NURBS-based model was built with extracted features points from origin subject. The model was sent for designer as well as 3D printed, and the customized GCS was tested on the 3D printed calf to test the validity. The reason of not trying the GCS on real subject is that, the scanned human shapes are without clothing, and GCS will slightly change the circumferential shape of calf (from origin shape to more round). However, it's believed that the NURBS-based model can replace current models in finite elements analysis to predict the deformation responses under compressive garments.

6.Conclusion

In this work, a parameterized 3D model of human calves was proposed based on human anatomy and non-uniform rational B-splines method, aiming to provide accurate and efficient establishment of human calf model to facilitate customization of medical compression stockings. The proposed series of methods include re-sampling to obtain an explicit shape of the scanned calf,

circumferential profile analysis to find the crucial cross-sections according to current on-going standards, contour analysis to determine the feature points and data points arrangement, as well as control points calculation and surface construction of the NURBS surface. To illustrate the superiority of this calf modeling based on NURBS, an error index was introduced to evaluate the distortion between the NURBS surface as well as the origin scanned shape. Analysis of the error showed that, the proposed modeling based on NURBS provide minimal errors observed as $0.37\% \pm 0.03\%$, about an order of magnitude less than previous work. A customized design of MCS based on this model was conducted and proved as valid to provide gradient compression on the calf. Overall, this parametric modeling uses only very small amount of data but achieves a relatively high-accuracy modeling approach for human extremity characterization. It's suggested that the proposed model and method can highly boost size customization of MCSs, and will also inspire customization of other compression garments for other limbs.

Acknowledgement

Funding

This research was funded by the National Natural Science Foundation of China (Grant No. 12002085, 51603039), Innovation and Technology Commission, Hong Kong SAR Government (Grant No. ITP/041/19TP). The work was also sponsored by Shanghai Pujiang Program, and the Fundamental Research Funds for the Central Universities, the Key Laboratory of Textile Science and Technology (Donghua University), Ministry of Education, also by the 111 Project (BP0719035), as well as the Initial Research Funds for Young Teachers of Donghua University.

Conflicts of interest

All authors of this work have no commercial or associative interest to declare that represents a conflict of interest in connection with this manuscript

submitted.

Statements of ethical approval

Ethical approval was obtained from the Research Ethics Committee of The Hong Kong Polytechnic University.

Availability of data and material

The raw/processed data required to reproduce these findings cannot be shared at this time as the data also forms part of an ongoing study.

Reference

[1]. Jida Huang, Tsz-Ho Kwok, and Chi Zhou, *Parametric design for human body modeling by wireframe-assisted deep learning.* Computer-Aided Design, 2019. **108**: p. 19-29.

[2]. Fabien Bernard, Mohsen Zare, Jean-Claude Sagot, and Raphael Paquin, *Using digital and physical simulation to focus on human factors and ergonomics in aviation maintainability.* Human factors, 2020. **62**(1): p. 37-54.

[3]. Chenxi Li and Fernand Cohen, *Virtual reconstruction of 3D articulated human shapes applied to garment try-on in a virtual fitting room.* Multimedia Tools and Applications, 2022. **81**(8): p. 11071-11085.

[4]. Miguel Martínez-García, Yu Zhang, and Timothy Gordon, *Memory pattern identification for feedback tracking control in human–machine systems.* Human factors, 2021. **63**(2): p. 210-226.

[5]. Xiuqin Shang, Fei-Yue Wang, Gang Xiong, Timo R Nyberg, Yong Yuan, Sheng Liu, Chao Guo, and Sen Bao, *Social manufacturing for high-end apparel customization.* IEEE/CAA Journal of Automatica Sinica, 2018. **5**(2): p. 489-500.

[6]. Łukasz Markiewicz, Marcin Witkowski, Robert Sitnik, and Elżbieta Mielicka, *3D anthropometric algorithms for the estimation of measurements required for specialized garment design.* Expert Systems with Applications, 2017. **85**: p. 366-385.

[7]. Alexander Wolf, Jörg Miehling, and Sandro Wartzack, *Challenges in interaction modelling with digital human models–A systematic literature review of interaction modelling approaches.* Ergonomics, 2020. **63**(11): p. 1442-1458.

[8]. Ying Xiong and Xiaoming Tao, *Compression garments for medical therapy and sports.* Polymers, 2018. **10**(6): p. 663.

[9]. Yoann Dessery and Jari Pallari, *Measurements agreement between low-cost and high-level handheld 3D scanners to scan the knee for designing a 3D printed knee brace.* PloS one, 2018. **13**(1): p. e0190585.

[10]. Ali Zine El-Abidine Arab, Ali Merdji, Ali Benaissa, Sandipan Roy, Bel-Abbes Bachir Bouiadjra, Khaled Layadi, Abdelhakim Ouddane, and Osama M Mukdadi, *Finite-element analysis of a lateral femoro-tibial impact on the total knee arthroplasty.* Computer methods and programs in biomedicine, 2020. **192**: p. 105446.

[11]. Orlando Adas Saliba Junior, Hamilton Almeida Rollo, Orlando Saliba, and Marcone Lima Sobreira, *Compression stocking prevents increased venous retrograde flow time in the lower limbs of pregnant women.* Phlebology, 2020. **35**(10): p. 784-791.

[12]. Robert R Attaran and Cassius I Ochoa Chaar, *Compression therapy for venous disease.* Phlebology, 2017. **32**(2): p. 81-88.

[13]. Markus Stücker, Olivia Danneil, Martin Dörler, Maren Hoffmann, Elena Kröger, and Stefanie Reich-Schupke, *Safety of a compression stocking for patients with chronic venous insufficiency (CVI) and peripheral artery disease (PAD).* JDDG: Journal der Deutschen Dermatologischen Gesellschaft, 2020. **18**(3): p. 207-213.

[14]. Hafiz Faisal Siddique, Adnan Ahmed Mazari, Antonin Havelka, Zdenek Kus, and Engin Akcagun, *Washing Characterization of Compression Socks.* Autex Research Journal, 2022.

[15]. Gyozo Szolnoky, Henriette Gavallér, Anna Gönczy, Imre Bihari, Lajos Kemény, Tamás Forster, and Attila Nemes, *The effects of below-knee medical compression stockings on pulse wave velocity of young healthy volunteers.* The Journal of Strength & Conditioning Research, 2021. **35**(1): p. 275-279.

[16]. Jie Pei, Huiju Park, and Susan P Ashdown, *Female breast shape categorization based on analysis of CAESAR 3D body scan data.* Textile Research Journal, 2019. **89**(4): p. 590-611.

[17]. Yue Sun, Kit-lun Yick, Winnie Yu, Lihua Chen, Newman Lau, Wanzhong Jiao, and Shichen Zhang, *3D bra and human interactive modeling using finite element method for bra design.* Computer-Aided Design, 2019. **114**: p. 13-27.

[18]. Mohammad Farukh Hashmi, B Kiran Kumar Ashish, Avinash G Keskar, Neeraj Dhanraj Bokde, and Zong Woo Geem, *FashionFit: Analysis of mapping 3D pose and neural body fit for custom virtual try-on.* IEEE Access, 2020. **8**: p. 91603-91615.

[19]. Rong Liu, Xia Guo, Qiujin Peng, Le Zhang, Terence T Lao, Trevor Little, Jundong Liu, and Eric Chan, *Stratified body shape-driven sizing system via three-dimensional digital anthropometry for compression textiles of*

lower extremities. Textile Research Journal, 2018. **88**(18): p. 2055-2075.
[20]. Shumi Zhao, Rong Liu, Chengwei Fei, and Dong Guan, *Dynamic interface pressure monitoring system for the morphological pressure mapping of intermittent pneumatic compression therapy.* Sensors, 2019. **19**(13): p. 2881.
[21]. Chia-Chen Kuo, Mao-Jiun Wang, and Jun-Ming Lu, *Developing sizing systems using 3D scanning head anthropometric data.* Measurement, 2020. **152**: p. 107264.
[22]. Abid Haleem and Mohd Javaid, *3D scanning applications in medical field: a literature-based review.* Clinical Epidemiology and Global Health, 2019. **7**(2): p. 199-210.
[23]. Zhi-Quan Cheng, Yin Chen, Ralph R Martin, Tong Wu, and Zhan Song, *Parametric modeling of 3D human body shape—A survey.* Computers & Graphics, 2018. **71**: p. 88-100.
[24]. Bharat Lal Bhatnagar, Cristian Sminchisescu, Christian Theobalt, and Gerard Pons-Moll. *Combining implicit function learning and parametric models for 3d human reconstruction*. in *European Conference on Computer Vision*. 2020. Springer.
[25]. Wang Xi, Yang Bao, Li Qiao, Guo Xia, and Tao Xiaoming, *Parametric modeling the human calves for evaluation and design of medical compression stockings.* Computer Methods and Programs in Biomedicine, 2020. **194**: p. 105515.
[26]. Tian-Xiang Yue, *Surface modeling: high accuracy and high speed methods*. Vol. 2. 2011: CRC press.
[27]. Yin Chen, Zhan Song, Weiwei Xu, Ralph R Martin, and Zhi-Quan Cheng, *Parametric 3D modeling of a symmetric human body.* Computers & Graphics, 2019. **81**: p. 52-60.
[28]. Aymen Mir, Thiemo Alldieck, and Gerard Pons-Moll. *Learning to transfer texture from clothing images to 3d humans*. in *Proceedings of the IEEE/CVF Conference on Computer Vision and Pattern Recognition*. 2020.
[29]. Riccardo Marin, Simone Melzi, Emanuele Rodola, and Umberto Castellani. *Farm: Functional automatic registration method for 3d human bodies*. in *Computer Graphics Forum*. 2020. Wiley Online Library.
[30]. Misato Kinoshita, Yuko Kurosawa, Sayuri Fuse, Riki Tanaka, Nobuko Tano, Ryota Kobayashi, Ryotaro Kime, and Takafumi Hamaoka, *Compression Stockings Suppressed Reduced Muscle Blood Volume and Oxygenation Levels Induced by Persistent Sitting.* Applied Sciences, 2019. **9**(9): p. 1800.
[31]. Bailin Deng, Yuxin Yao, Roberto M. Dyke, and Juyong Zhang, *A Survey of Non-Rigid 3D Registration.* Computer Graphics Forum, 2022. **41**(2): p. 559-589.
[32]. Orest Mykhaskiv, Mladen Banović, Salvatore Auriemma, Pavanakumar

Mohanamuraly, Andrea Walther, Herve Legrand, and Jens-Dominik Mü ller, *NURBS-based and parametric-based shape optimization with differentiated CAD kernel.* Computer-Aided Design and Applications, 2018. **15**(6): p. 916-926.

[33]. Sergey N Makarov, Gregory M Noetscher, Janakinadh Yanamadala, Matthew W Piazza, Sara Louie, Alexander Prokop, Ara Nazarian, and Aapo Nummenmaa, *Virtual human models for electromagnetic studies and their applications.* IEEE reviews in biomedical engineering, 2017. **10**: p. 95-121.

[34]. Aakash Soni, Sachin Kumar, and Navin Kumar, *Stochastic failure analysis of proximal femur using an isogeometric analysis based nonlocal gradient-enhanced damage model.* Computer Methods and Programs in Biomedicine, 2022. **220**: p. 106820.

[35]. Matthew JianQiao Peng, XiongWei Cao, Hai-Yan Chen, Yong Hu, XinXu Li, YongQiang Lao, and Bo Bai, *Intralesional curettage versus prosthetic replacement for bone tumors—a finite element analysis case of limb salvage simulation in biomechanics.* Computer Methods and Programs in Biomedicine, 2021. **198**: p. 105775.

[36]. Chen Feng and Yuichi Taguchi, *FasTFit: A fast T-spline fitting algorithm.* Computer-Aided Design, 2017. **92**: p. 11-21.

[37]. Carlotta Giannelli, Bert Jüttler, Stefan K. Kleiss, Angelos Mantzaflaris, Bernd Simeon, and Jaka Špeh, *THB-splines: An effective mathematical technology for adaptive refinement in geometric design and isogeometric analysis.* Computer Methods in Applied Mechanics and Engineering, 2016. **299**: p. 337-365.

[38]. Penguian. *NURBS Toolbox by D.M. Spink*. 2021 [cited 2022 July 25]; MATLAB Central File Exchange]. Available from: https://www.mathworks.com/matlabcentral/fileexchange/26390-nurbs-toolbox-by-d-mspink.

[39]. Ilijas Selimovic, *Improved algorithms for the projection of points on NURBS curves and surfaces.* Computer Aided Geometric Design, 2006. **23**(5): p. 439-445.